

High-resolution atomic absorption spectrometry combined with machine learning data processing for isotope amount ratio analysis of lithium

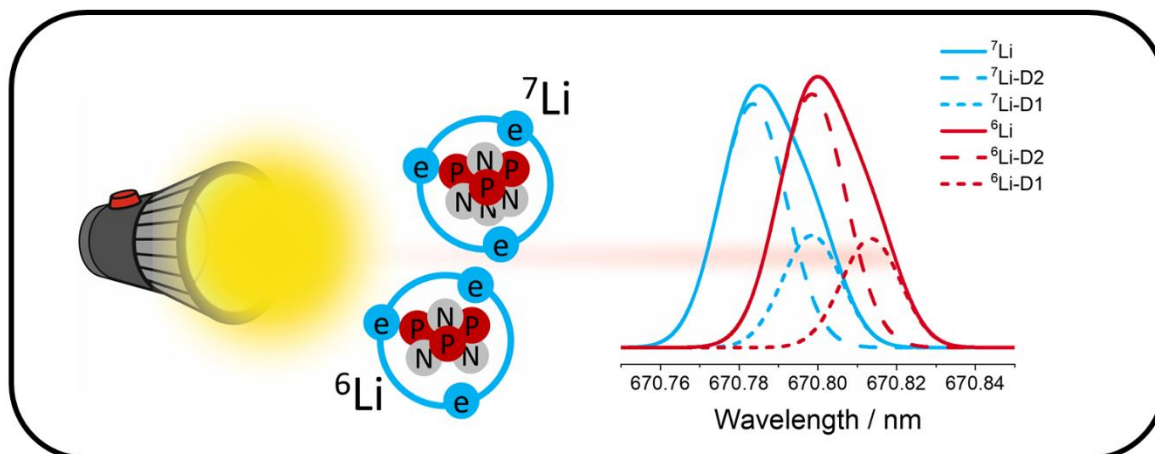
Alexander Winckelmann^{1,2}, Sascha Nowak³, Silke Richter², Sebastian Recknagel², Jens Riedel², Jochen Vogl², Ulrich Panne^{1,2}, Carlos Abad^{2*}

¹Humboldt-Universität zu Berlin, Department of Chemistry, Brook-Taylor-Str. 2, 12489 Berlin, Germany

²Bundesanstalt für Materialforschung und –prüfung (BAM), Richard-Willstätter-Str. 11, 12489 Berlin, Germany

³MEET Battery Research Center, University of Münster, Corrensstr. 46, 48149 Münster, Germany

*E-mail corresponding author: carlos.abad@bam.de



Data Analysis
by Machine Learning



$$\delta^{7/6}\text{Li} = \left[\frac{\left(\frac{{}^7\text{Li}}{{}^6\text{Li}} \right)_{\text{Sample}}}{\left(\frac{{}^7\text{Li}}{{}^6\text{Li}} \right)_{\text{Standard}}} \right] - 1$$

Abstract

An alternative method for lithium isotope amount ratio analysis based on a combination of high-resolution atomic absorption spectrometry and spectral data analysis by machine learning (ML) is proposed herein. It is based on the well-known isotope shift of approximately 15 pm for the electronic transition $2^2P \leftarrow 2^2S$ at around the wavelength of 670.8 nm, which can be measured by state-of-the-art high-resolution continuum source graphite furnace atomic absorption spectrometry. For isotope amount ratio analysis, a scalable tree boosting ML algorithm (XGBoost) was employed and calibrated using a set of samples with ^6Li isotope amount fractions ranging from 0.06 to 0.99 mol mol⁻¹, previously determined by multi-collector inductively coupled plasma mass spectrometry (MC-ICP-MS). The calibration ML model was validated with two certified reference materials (LSVEC and IRMM-016). The procedure was applied to the isotope amount ratio determination of a set of stock chemicals (Li_2CO_3 , LiNO_3 , LiCl , and LiOH) and a BAM candidate reference material, that is, $\text{LiNi}_{1/3}\text{Mn}_{1/3}\text{Co}_{1/3}\text{O}_2$ (NMC111) cathode material. The results of these determinations were compared with those obtained by MC-ICP-MS and found to be metrologically comparable and compatible. The residual bias was -1.8‰ and the precision obtained ranged from 1.9‰ to 6.2‰. This precision was sufficient to resolve naturally occurring variations, as demonstrated for samples ranging from approximately -3‰ to $+15\text{‰}$. To assess its suitability to technical applications, the NMC111 cathode candidate reference material was analyzed using high-resolution continuum source molecular absorption spectrometry with and without matrix purification. The results obtained were metrologically compatible with each other.

1. Introduction

Lithium is a widely occurring, light element in the Earth's crust. It possesses two naturally occurring isotopes, ^6Li and ^7Li . Owing to their relatively large mass difference ($\approx 16\%$), even a very small amount of isotopic fractionation leads to significant isotope ratio differences. The study of Li isotope fractionation has been used to explain many Earth surface processes, for example, as a tracer of crustal recycling¹ or (reverse) weathering reactions.^{2,3} Additionally, Li isotope fractionation may be used to obtain a better understanding of Li-ion transfer and determination of electrochemically active lithium

loss in lithium ion batteries.⁴ It is crucial for the understanding of the aging mechanisms and therefore leading to the improved design of long-lasting batteries.^{5,6}

Presently, mass spectrometry (MS) is considered the standard technique for Li isotope ratio analysis. Since the introduction of highly precise TIMS procedures⁷ in 1988 and multi-collector inductively coupled plasma mass spectrometry (MC-ICP-MS) procedures in 1999,⁸ many MS methods for Li isotope amount ratios have been proposed.⁹ However, elemental MS of Li is not without potential pitfalls. Owing to the low mass-to-charge ratio of Li and the resulting high relative mass difference between its two isotopes, MS methods are prone to large mass bias effects and strong matrix interferences that directly affect both trueness and precision.¹⁰ Therefore, laborious and complicated matrix extraction procedures must be followed.¹¹ Although chromatographic separation has been automated recently,¹² the chemical separation produces large amounts of waste, requires expensive equipment, and takes several hours. An instrumental alternative to MS analysis has therefore long been anticipated, with optical spectrometry being the most promising candidate.¹³

The isotopic shift in the electronic spectrum of atoms and diatomic molecules (primary isotope effect) enables isotope analysis with moderate-resolution instruments in the ultraviolet/visible spectral range. Although first described more than 100 years ago,¹⁴ optical spectrometry for isotope ratio analysis has long lagged behind MS owing to its lack of sensitivity and precision. However, in recent years, this situation has developed. Better optical spectrometers and more sensitive detectors have been developed;^{15,16} moreover, improved computing possibilities for machine learning (ML) and artificial intelligence algorithms have become available.¹⁷ These algorithms may not resolve the complex electronic atomic structure, but they can identify the relationship between the isotopic composition and electronic spectra of a given sample.

With the development of atomic absorption spectrometry (AAS), Sir Alan Walsh suggested the potential for isotope analysis by this optical method based on the monitoring of the isotopic shift in atomic lines.¹⁸ This principle was applied successfully by comparing the absorbance of hollow cathode lamps made of natural and enriched Li.¹⁹ This approach was further investigated by the simultaneous absorbance

measurements of natural and enriched hollow cathode lamps using dual beams.²⁰ Such a setup achieved absolute uncertainties of 0.005 mol mol⁻¹ for measurements of isotope amount fractions. Various attempts were made to minimize the Li concentration dependence using nonlinear equations²¹ or extrapolating the Li content/absorbance ratios,²² with uncertainties of 0.006 and 0.007 mol mol⁻¹ achieved, respectively. The use of diode lasers in absorption and fluorescence spectrometry made it possible to separate ⁶Li and ⁷Li in the atomic spectra.^{23,24} Isotope amount ratios can therefore be determined with uncertainties of 1% to 4%. The combination of absorption and emission spectrometry is also possible, eliminating the need for enriched hollow cathode lamps.²⁵ However, with these methods, the uncertainties are too large to differentiate between samples with naturally occurring isotopic compositions, showing a variation ranging from -20‰ to +80‰ versus the internationally accepted delta zero standard LSVEC (NIST SRM 8545).²⁶

During the last decade, high-resolution optical spectrometry has been proposed for isotope analysis by either applying molecular emission spectrometry, laser ablation molecular isotopic spectrometry,²⁷ or high-resolution continuum source molecular absorption spectrometry (HR-CS-MAS), wherein the isotope shift is larger in diatomic molecules than it is in atoms.²⁸ By combination with the chemometric analysis of spectral data, these methods can potentially mature into fast, low-cost alternatives for isotopic research. By using HR-CS-MAS, molecular spectral analysis of diatomic molecules has also been applied to elemental trace analysis via isotope dilution molecular absorption spectrometry. Using high-resolution continuum source graphite furnace molecular absorption spectrometry (HR-CS-GF-MAS), a graphite furnace can be used as a chemical reactor for the generation of a diatomic molecule. For example, Cl has been quantified based on the isotope shift and relative intensities of the isotopologue couple Al³⁵Cl/Al³⁷Cl and by adding isotopic spikes.²⁹ The same procedure was used for Br trace analysis by monitoring the isotopologue couple Ca⁷⁹Br/Ca⁸¹Br,³⁰ and for Ca trace analysis using the couple ⁴⁴CaF/⁴⁰CaF.³¹

Our group's recent research proposed the determination of B isotope amount ratios by combining the spectral data from boron hydride (BH) measurements by HR-CS-GF-MAS and multivariate analysis.³²

A partial least squares regression (PLS-R) made from a BH molecular spectra library with different $^{11}\text{B}/^{10}\text{B}$ fractions was used, and precision between 0.013% and 0.05% was reported. This precision is sufficiently small to allow the monitoring of natural B isotopic variations.

However, there is not yet a suitable Li molecule that enables isotope analysis. Nevertheless, the atomic spectroscopy of Li can be an attractive alternative owing to its sensitivity and the large, measurable isotopic shift. Preliminary results by Cramers et al. proposed the isotope analysis of Li by laser-induced breakdown spectroscopy and chemometric calibration based on the atomic spectra at around 670 nm using a double echelle modular spectrometer (DEMON).¹⁵ In the present work, atomic lines were studied using HR-CS-GF-AAS, a softer atomization method than a laser-induced plasma. HR-CS-AAS instruments include a DEMON spectrometer capable of partially resolving the atomic lines of Li. The application of advanced chemometric techniques with predetermined reference data in the calibration for sample analysis was evaluated in the present work and compared with a highly precise and accurate isotope ratio analysis method, that is, MC-ICP-MS.

Modern computational and data science provide new alternatives for data analysis, for example, tree boosting methods, in which an algorithm learns from small differences in a given dataset with more accuracy.³³ Tree boosting is a highly effective ML branch that is used widely by data scientists. Extreme gradient boosting (XGBoost) is a sparsity-aware algorithm for sparse data and a weighted quantile sketch for approximate tree learning. It provides insights on cache access patterns, data compression, and database fragmenting to build a scalable tree boosting system. XGBoost has higher predictive power than other ML techniques and also includes regularization, which reduces overfitting and improves overall performance. Hence, it is also known as a “regularized boosting” method suitable for spectral and chemical analyses.^{34,35} With recent innovations in ML, we can further improve data analyses and achieve unrivaled precision in isotope analyses using optical spectrometry.

A direct comparison was performed to compare the suitability of atomic absorption/ML as a practical alternative to ICP-MS. The study covers a variety of samples, encompassing a wide range of isotope

amount ratios and matrices. To fully exploit the ML approach's capabilities, the results obtained in the ICP experiments were also used for the training and validation of the ML algorithm.

2. Experimental Section

2.1. Sample preparation

High-purity deionized water with a resistivity of 18 M Ω cm from a Milli-Q system (Millipore gradient, Merck Millipore, Darmstadt, Germany) was used throughout the experiments. Hydrochloric and nitric acids (EMSURE®, Merck, Darmstadt, Germany) were used after purification by sub-boiling distillation in PFA containers. The samples analyzed consisted of a Li cathode material (LiNMC) (BAM candidate reference material; a mixture of Li, Mn, Ni, and Co oxides), lithium carbonate (TraceSELECT®, Fluka), lithium chloride, and lithium hydroxide (Merck, Darmstadt, Germany). All materials were of p.a grade. The preparations are shown in Table S1. For calibration of the AAS measurements, solutions of different Li isotope amount ratios were prepared by combining a Li ICP standard (Certipur®, Merck, Darmstadt, Germany) and a ^6Li standard solution prepared at BAM. Additionally, a lithium fluoride material (p.a grade; Merck, Darmstadt, Germany) was employed in the calibration owing to its extreme non-natural delta value, which helped in the training of the ML algorithm ($\delta^7\text{Li}_{\text{LSVEC}} = 294.82\text{‰} \pm 0.89\text{‰}$). Certified reference materials (CRMs) were used in the calibration and validation: LSVEC, a lithium carbonate that is the internationally accepted delta zero standard NIST SRM 8545 (NIST, Gaithersburg, MD, USA), and the CRM lithium carbonate, IRMM-016 (European Commission JRC, Belgium).

The lithium ion battery cathode material was separated into five fractions of approximately 100 mg each (samples A1 to A5) and dissolved in aqua regia. The Li was extracted quantitatively by ion-exchange chromatography (IC) on a column filled with 3 mL of AG-50W-X8 resin (analytical grade, BIO-RAD). This matrix separation is the modified procedure of Van Hoecke et al.¹¹ (Tables S4, S5). All samples were prepared using the same diluted nitric acid ($w(\text{HNO}_3) = 20 \text{ g kg}^{-1}$).

2.2. Measurements using ICP-optical emission spectrometry

Before measurements using MS and HR-CS-GF-AAS, the Li concentrations of the samples were determined using ICP-optical emission spectrometry (OES) with an Agilent 5110 ICP-OES with an automatic sampling system (SPS 4) (Agilent Technologies Australia Pty Ltd, Australia). Direct calibration from 20 to 1000 $\mu\text{g L}^{-1}$ Li was performed at a wavelength of 670.783 nm in axial mode using certified single-element stock solutions, a Li ICP Standard (Certipur®), or an ICP multi-element standard solution (IV Certipur®) depending on the matrix of the sample. The instrument parameters are given in Table S2.

2.3. Measurements using MS

2.3.1 General procedure

The Li delta values and isotope amount ratios were measured using a Neptune Plus MC-ICP-MS instrument (Thermo Fisher Scientific, Bremen, Germany) in standard configuration. The corresponding instrument parameters are listed in Table S3. With a Li mass fraction of approximately 0.5 mg kg⁻¹, an average signal intensity of 12 V for Li was obtained and a typical repeatability of approximately 0.1‰ for Li isotope ratio measurements was observed. As the standard in δ -measurements, the standard–sample bracketing approach was applied, with a blank measurement before each standard and before each sample.

Each sample was measured at least three times. The typical drift in the ⁷Li/⁶Li ratio was 0.1‰ to 0.2‰, as observed by two consecutive bracketing standard measurements of LSVEC during the sequences. Each sample was measured with 50 cycles, with outliers identified based on the twofold standard deviation ($2s$) criterion and removed from the dataset. Blank correction for the outlier-corrected intensities was performed by subtracting the average intensities from the preceding and subsequent blanks. Calculations and corrections were made within the measurement sequence by the Thermo Scientific Neptune software. The preceding and following standards of each sample measurement were averaged and the δ -value of the sample calculated according to Equation 1, with \bar{R} being the average

ratio of the preceding and subsequent standards. The bracketing standard was LSVEC; therefore, delta values were obtained on the LSVEC delta scale.

$$\delta^7Li = \delta^{7/6}Li_{LSVEC} = \left(\frac{R_{Smp}^{meas}\left(\frac{^7Li}{^6Li}\right)}{\bar{R}_{LSVEC}^{meas}\left(\frac{^7Li}{^6Li}\right)} \right) - 1 \text{ Eqn. 1}$$

All samples and standards were diluted with the same diluted nitric acid ($w(\text{HNO}_3) = 20 \text{ g kg}^{-1}$) such that an intensity matching of better than $\pm 10\%$ was achieved. As a quality control LSVEC was measured twice as a sample and yielded δ^7Li values of 0.11‰ and 0.04‰, which agreed well with the target value of 0‰ within the standard uncertainty of 0.25‰.

Measurement uncertainties were calculated based on an approach invented by Rosner et al.,³⁶ which applies a modified δ -equation for TIMS measurements. This approach has been further improved for MC-ICP-MS measurements.³⁷

The measurement uncertainties were calculated using the software tool GUM Workbench (Metrodata 2019, Version 2.4.1.375, Metrodata GmbH, Braunschweig, Germany). Combined δ^7Li standard uncertainties (u_c) of 0.25‰ to 0.27‰ were obtained for unprocessed samples (e.g., dissolved Li_2CO_3) and of 0.32‰ to 0.41‰ for processed (matrix separated) samples. The combined measurement uncertainty was calculated for each individual δ -value and converted to an expanded uncertainty U with a coverage factor of two.

2.3.2. Measurements of calibration standards for AAS

Isotope amount ratios were measured in separate sequences in blocks of three standards and three samples in alternating order, each separated by two blank measurements. This sequence was applied because isotopically enriched solutions were measured, and any carry-over effect should be minimized. The measured ion intensity ratios were corrected for mass bias by multiplying by a correction factor calculated from the isotope amount ratios of LSVEC³⁸ divided by the measured ion intensity ratios of

LSVEC. Measurement uncertainties were calculated accordingly. Isotope amount ratios can also be calculated from the $\delta^7\text{Li}$ values and the isotope amount ratio of LSVEC and its associated uncertainty.³⁸

2.4. Measurements using HR-CS-GF-AAS

A model contraAA 800D HR-CS-AAS (Analytik Jena, Germany) with GF (PIN platform) was used for all experiments. The instrument's wavelength was set to 670.7845 nm and the optimized temperature program given in Table 1 was used. Argon N5.0 (Air Liquide, Krefeld, Germany) was used as the primary gas. A mixture of 1 % trifluoromethane N5.0 in Ar (GHC Gerling, Holz & Co., Hamburg, Germany) was used as the secondary gas to avoid the formation of lithium carbides and a subsequent memory effect.³² A volume of 10 μL of each sample with a Li mass concentration of 25 $\mu\text{g L}^{-1}$ was injected for each measurement.

Table 1. Temperature program for lithium atomization

Step	Name	Temp	Ramp	Hold	Time	Gas flow	
		/ $^{\circ}\text{C}$	/ $^{\circ}\text{C s}^{-1}$	/ s	/ s	Primary / L min^{-1}	Secondary / L min^{-1}
1	Dry	70	6	15	22.5	2.0	-
2	Dry	80	6	20	21.7	2.0	-
3	Dry	90	3	20	23.3	2.0	-
4	Dry	110	5	10	14.0	2.0	-
5	Pyrolysis 1	350	50	20	24.8	2.0	-
6	Pyrolysis 2	750	300	10	11.3	0.1	-
7	Gas adaption	750	0	5	5.0	-	-
8	Atomization	2350	1500	10	11.0	-	-
9	Clean out 1	2450	500	10	10.2	-	0.5
10	Clean out 2	2600	500	4	4.3	2.0	-

Each sample was measured 10 times and 150 spectra were recorded for each measurement. An extinction maximum of approximately 0.6 was observed. Between each sample, a blank sample was measured five times. At wavelengths of 323.2657 and 274.1200 nm, samples with a Li concentration of 0.5 mg L^{-1} were analyzed; extinction maxima of approximately 0.04 and 0.05 were observed, respectively. In a

bracketing approach, samples and LSVEC standards were injected three times in alternating order with one blank injection between each.

The wavelengths of 323.2657 and 274.1200 nm were evaluated. Although these secondary atomic absorption wavelengths presented a measurable isotope shift (around 4 pm), the echelle spectrometer's resolution used for this wavelength region was higher than that for the wavelength region of around 670.78 nm. They were not used for isotope analysis because of the low signal-to-noise ratio.

2.5. Data analysis using ML

Isotope amount ratios were determined using a scalable tree boosting system (XGBoost algorithm).³³ Time-resolved 3D spectral data (baseline background corrected) acquired using the HR-CS-AAS instrument were exported using the Aspect CS 2.2.1.0 software (Analytik Jena AG). For each measurement, 150 spectra were collected during the atomization. Prior to analysis by ML, spectral data were preprocessed and reduced in MATLAB (R2020a, The MathWorks Inc., USA). A blank was subtracted from each measurement before it was compiled, transformed, and integrated from a 3D spectrum to a 2D spectrum by converting to its spectra average. Finally, the isotope amount ratio analysis was performed using MATLAB-based stand-alone software SOLO+MIA, version 8.9, 2020 (Eigenvector, Inc., USA).³⁹ The SOLO+MIA software integrated the XGBoost regression algorithm.

An XGBoost regression starts with an initial prediction, after which a loss function is used to evaluate whether the prediction worked well. A dataset contains n number of spectra or isotopic patterns (an isotopic combination used for training), which means n rows, and uses i to represent each constituent spectrum. XGBoost uses a loss function to build trees to minimize Equation 2, as described by Chen and Guestrin.³³

$$\mathcal{L}(\phi) = \sum_i \ell(\hat{y}_i, y_i) + \sum_k \Omega(f_k) \text{ Eqn. 2}$$

$$\text{where } \Omega(f) = \gamma T + \frac{1}{2} \lambda \|w\|^2$$

Equation 2 represents the loss function of the decision's tree, and for each leaf, calculates the pseudo residuals of the predicted value (\hat{y}_i) and the true value (y_i). The omega component contains the regularization term lambda (λ), where w represents the leaf weight (it could also be considered the output value for the leaf). The regularization is intended to reduce underestimation or overfitting of individual observations. T represents the number of terminal nodes or leaves in a tree and gamma (γ) represents the user-definable penalty for pruning.

An ML analysis procedure by the XGBoost algorithm is summarized in the flow diagram of Fig. 1. A learning calibration model was constructed with the calibration samples K00 to K10, sample A10, and reference materials LSVEC and IRMM-016 (spectra in predictor block or X-block), covering ^6Li isotope amount fractions from 0.06 to 0.99 mol mol⁻¹. The analysis range (variables) was set between wavelengths of 670.631 and 670.934 nm. The data were preprocessed by a principal component regression (PC-R) to reduce the number of dimensions. The absolute isotope composition measured using MC-ICP-MS (in the calibration samples) of these samples or the certified samples in the reference materials was used for calibration (isotopic amount fraction composition used in the predicted block or Y-block).

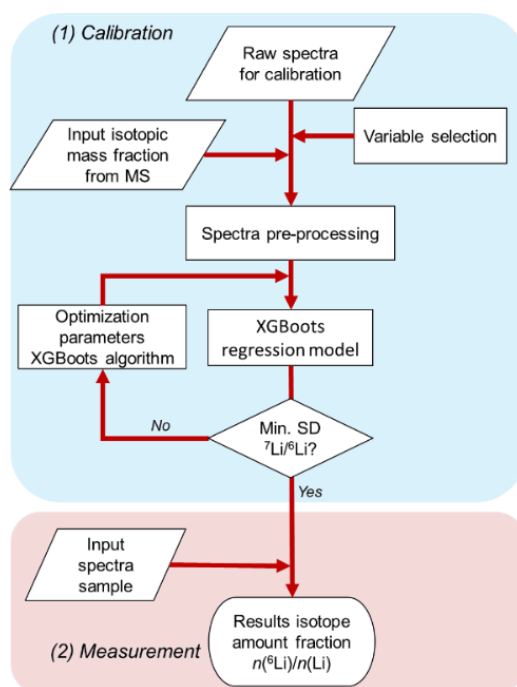


Fig. 1. Flow diagram for the spectral data analysis using machine learning.

The isotope ${}^6\text{Li}$ was selected as the target isotope as the algorithm used in the SOLO+MIA program processes only one variable in the Y-block. Fully optimized parameters were achieved by reaching a minimum standard deviation for the CRMs. The optimized parameters are shown in Table 2. The results obtained from the XGBoost algorithm corresponded to the ${}^6\text{Li}$ isotope amount fraction. The ${}^7\text{Li}$ isotope amount fraction was calculated as unity reduced by the ${}^6\text{Li}$ isotope amount fraction (Equation 3).

$$\frac{n \text{ } ^7\text{Li}}{n\text{Li}} = 1 - \frac{n \text{ } ^6\text{Li}}{n\text{Li}} \text{ Eqn. 3}$$

Table 2. Optimized parameters for the spectral analysis using an XGBoost algorithm

Parameter	Value
Preprocessing spectra (X-block)	Three steps: 1) Normalization area = 1 2) 2 nd derivative Savitzky–Golay (order 2, window 15 points, tails weighted) 3) Mean center
Preprocessing isotopic composition (Y-block)	Mean center
Target isotope	${}^6\text{Li}$
Compression spectral data (X-block)	PC-R with 6 latent variables
Mahalanobis distance corrected scores for compression model	none
Algorithm	xgboost
Booster	gbtree
Evaluation metric	rmse
Objective	reg:linear
Eta (learning rate)	0.001
Maximal depth	6
Number of rounds	30000
Alpha	0
Gamma	0
Lambda	0
Scale_pos_weight	1
Cross-validation	Venetian blinds with 10 splits and blind thickness = 1
RMSEC	9.23×10^{-5}
Bias	6.27×10^{-9}

R ² calibration	1
R ² cross-validation	1

3. Results and Discussion

3.1. Isotope shift in atomic spectra

The most suitable atomic line for isotope analysis corresponded to the electronic transition $2^2P \leftarrow 2^2S$, which was found at around the 670.8-nm wavelength (Fig. 2A). Compared with other electronic transitions, this absorption line is convenient owing to its isotopic shift (15 pm), being at least one order of magnitude larger than other explored electronic transitions (4 pm for 323.2657 and 274.1200 nm). The high sensitivity of this electronic transition allowed for the analyses of samples in the ultra-trace concentration range (characteristic concentration (m_c) for Li in graphite furnace is 0.6 μg). However, the isotope shift in the $2^2P \leftarrow 2^2S$ transition did not present a linear correlation with its isotopic composition (Fig. 2B). This is because of the fine structure splitting between the $2^2P_{1/2}$ and $2^2P_{3/2}$ components (a doublet), such that the transitions in the fine structure, $^7\text{Li-D}_1$ and $^6\text{Li-D}_2$ corresponding to $2^2P_{1/2} \leftarrow 2^2S_{1/2}$ and $2^2P_{3/2} \leftarrow 2^2S_{1/2}$, respectively, overlapped (Fig. 2C).⁴⁰ For this reason, previously described optical methods for isotope amount ratio analyses based on the study of the electronic transition $2^2P \leftarrow 2^2S$ failed in terms of the precision and accuracy needed for isotope amount ratio analysis of naturally occurring samples, which are in the delta range of -20% to $+80\%$ vs. the LSVEC reference material.²⁶

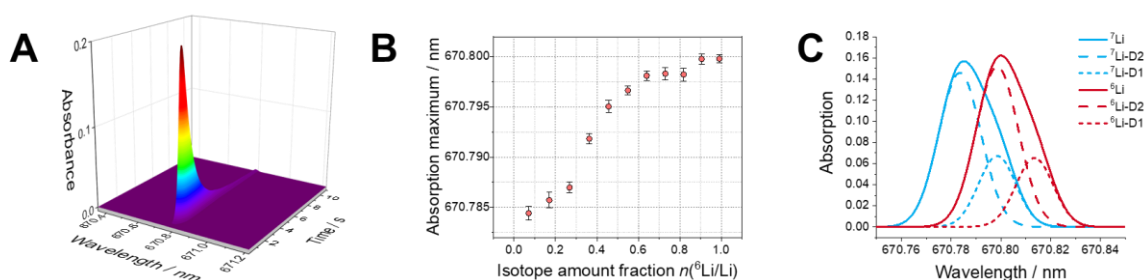


Fig. 2. (A) Time-resolved spectra for 10 μL of a 25 $\mu\text{g L}^{-1}$ Li solution (LSVEC) at around the 670.78-nm wavelength, as measured by HR-CS-GF-AAS. (B) Isotopic shift for the peak maximum for the atomic absorption line at around 670 nm, depending on its isotopic composition. Error bars represent the standard deviation of 10 measurements. The absorption maxima were determined by cubic spline data interpolation using the MATLAB spline function. (C) Blue curves: electronic transition $2^2P \leftarrow 2^2S$ for an enriched ^7Li solution (relative isotope amount fraction 99%) and the deconvolution by curve fitting of its fine

structure (D1 and D2 lines). Red curves represent the same electronic transition for an enriched ${}^6\text{Li}$ solution (relative isotope amount fraction 94%).

3.2. ML and optimization of parameters

Although the HR-CS-AAS instrument used a DEMON spectrometer with a resolution of approximately $140,000 \Delta\lambda/\lambda$,⁴¹ it was insufficient to completely resolve the Li isotope shift for the doublet in the electronic transition $2^2\text{P} \leftarrow 2^2\text{S}$ (Figs. 2C and 3A). Therefore, linear analyses methods fail in the spectral deconvolution and accurate differentiation of naturally occurring isotope differences. At present, standard chemometric methods such as principal component regression and PLS-R cannot deconvolute isotopic components with the desired accuracy.

For isotope analyses using the XGBoost algorithm, the calibration or supervised learning was planned with a predetermined dataset (samples measured previously using MS), as shown in Fig. 1. The analysis using ML involved two processes: (i) calibration (learning model) and (ii) validation / prediction. Validation of the ML model was made by cross-validation (Venetian blinds) and the two CRMs. Before analyzing and loading the algorithm with the spectral data obtained from HR-CS-GF-AAS (Fig. 3A), these data were preprocessed using a mathematical conversion to maximize the features and tiny changes in the atomic spectra so that the algorithm had more variations in learning (Fig. 3B). This preprocessing included (in order) area normalization, 2nd derivative, and mean center. Mean-centering calculates the mean of each variable and subtracts this from the dataset. The root mean-square error (RMSE) was used to estimate the best XGBoost model; the RMSE indicates when a minimum was reached in the optimization of the parameters shown in Table 2. Finally, in addition to the RMSE, the standard deviation of the learning samples (K00 to K10 and CRMs) was fine-tuned as a control parameter.

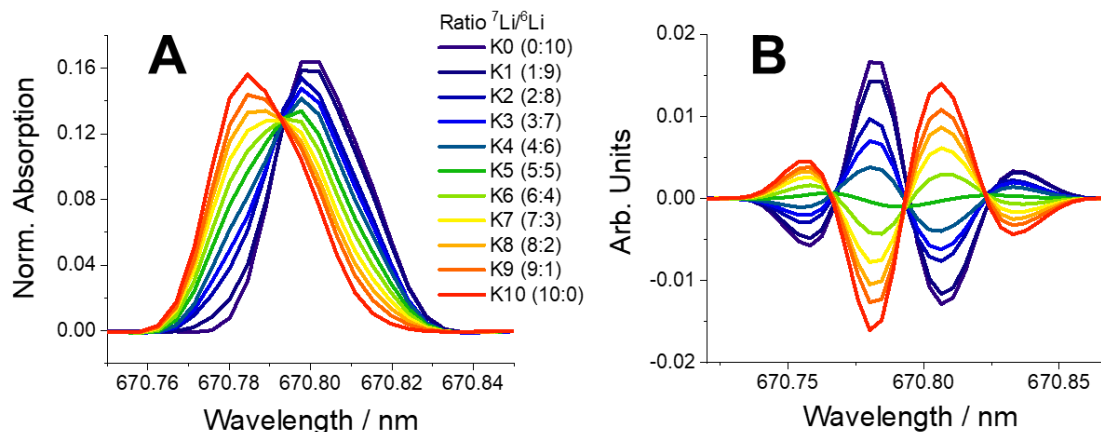


Fig. 3. (A) Spectra of Li (electronic transition 22P←22S) for different isotopic compositions. Exact isotopic compositions of the calibration samples K0 to K10 are shown in Table S1. (B) Magnification of spectral differences from (A) by mathematical processing, that is, area normalization, 2nd derivative, and mean center.

3.3. Isotope analysis

The target isotope for analysis using the XGBoost algorithm was ${}^6\text{Li}$. Variations of its isotope amount fractions (lines D₁ and D₂ in Fig. 2C) were more pronounced than those for ${}^7\text{Li}$; therefore, they were more effective in the XGBoost analysis. The isotope amount fraction of ${}^7\text{Li}$ was calculated using Equation 3, and delta values were calculated using Equation 1 vs. LSVEC. Results in the form of isotope amount fractions are shown in Table S6, and their conversion into delta scale vs. LSVEC are reported in Table 3. Detailed results for isotope amount ratios, isotope amount fractions, delta values, and molar masses measured using HR-CS-GF-AAS are reported in Table S6. To evaluate the trueness and precision of the results, the samples were additionally measured using MC-ICP-MS. These results are compared in Figs. 4A and 4B. The procedure presents a residual negative bias of -1.8‰ , which was calculated as the average of the deviation from the mass spectrometric values; it is taken as the method's trueness. This negative bias can be related to the overlapping of the fine atomic lines ${}^7\text{Li-D}_1$ and ${}^6\text{Li-D}_2$ (previously explained). The precision of the method developed ranged between 1.9‰ and 6.2‰ based on the maximal and minimal uncertainties (standard deviation of the mean $n = 10$ with a coverage factor of $k = 2$, corresponding to a level of confidence of 95%). The metrological compatibility of the HR-CS-AAS data with the MC-ICP-MS data was tested by applying the E_n value, which is the difference of two

values divided by the expanded uncertainty of this difference.^{42,43} For E_n values ≤ 1 , both values are metrologically compatible; for E_n values > 1 , neither value is metrologically compatible. The E_n values were calculated for all HR-CS-AAS data versus the corresponding MC-ICP-MS data and are displayed in Table 3. These values demonstrate metrological compatibility for all data except for sample A7, which presumably indicates an underestimated measurement uncertainty.

Table 3. Results for isotope analysis using HR-CS-GF-AAS

Sample	Material	$\delta^7\text{Li}$ vs. LSVEC / ‰						E_n	
		HR-CS-AAS (with IC separation)		HR-CS-AAS (without IC separation)		MC-ICP-MS		AAS with IC vs. MS	AAS without IC vs. MS
		Value	U^*	Value	U^*	Value	U		
A01	NMC111 cathode material	12.2	3.4	13.0	2.7	14.52	0.70	0.67	0.54
A02	NMC111 cathode material	13.4	6.2	13.1	1.9	14.68	0.69	0.21	0.78
A03	NMC111 cathode material	12.2	3.0	13.0	2.1	14.50	0.68	0.75	0.68
A04	NMC111 cathode material	12.2	2.4	13.1	2.1	14.63	0.66	0.98	0.70
A05	NMC111 cathode material	13.4	2.9	13.5	2.3	14.58	0.67	0.40	0.45
A06	Lithium carbonate	-	-	-1.3	3.6	-2.66	0.53		0.37
A07	Lithium carbonate	-	-	12.2	2.7	15.34	0.55		1.14
A08	Lithium chloride	-	-	4.8	3.7	5.21	0.55		0.11
A09	Lithium hydroxide	-	-	0.2	3.9	0.79	0.55		0.15

* Uncertainties are reported as the standard deviation of the mean ($n = 10$), with a coverage factor of $k = 2$, corresponding to a confidence level of 95%.

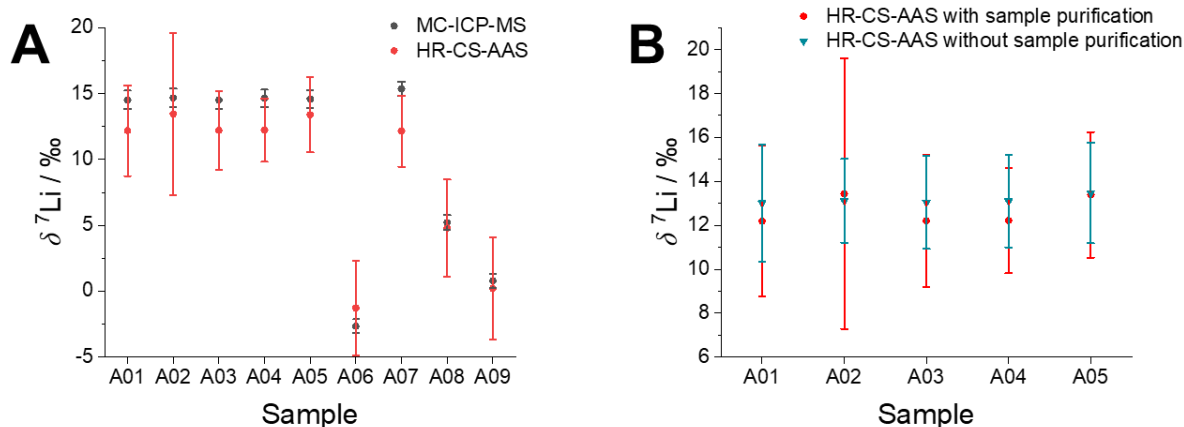


Fig. 4. (A) Comparison of $\delta^7\text{Li}$ vs. LSVEC measured using MC-ICP-MS and HR-CS-GF-AAS. (B) Comparison of $\delta^7\text{Li}$ vs. LSVEC for the Li cathode material with and without sample preparation (direct analysis) using HR-CS-GF-AAS.

Additional quality control measures were used for the two CRMs LSVEC and IRMM-016, which were applied previously as two of thirteen calibration standards. The values measured separately were $0.08200 \pm 0.00029 \text{ mol mol}^{-1}$ for IRMM-016 and $0.08209 \pm 0.00011 \text{ mol mol}^{-1}$ for LSVEC, with corresponding certified values of $0.082121 \pm 0.000087 \text{ mol mol}^{-1}$ for IRMM-016 and $0.08215 \pm 0.00023 \text{ mol mol}^{-1}$ for LSVEC (all data with expanded uncertainties). The resulting E_n values of 0.20 and 0.12 demonstrate metrological compatibility between the HR-CS-AAS data and the certified data.

Although the uncertainties were up to one order of magnitude larger than those obtained using MC-ICP-MS, the optical method proposed can distinguish naturally occurring variations between -20% and $+80\%$. Under the studied conditions, an analysis using sample bracketing with a CRM (LSVEC) did not improve trueness and precision.

As the spectral region around the 670-nm wavelength did not show any spectral interference for the sample studied (cathode material), this material was also analyzed without sample preparation by IC after acid digestion. The results obtained without separation were comparable and compatible with those obtained after IC matrix separation (Fig. 4B). This analysis demonstrates less matrix sensitivity than

ICP-MS, which has shown a bias of a few per mille in the $\delta^{11}\text{B}$ value for samples $\geq 10 \text{ mg kg}^{-1}$ of an artificial seawater matrix.⁴⁴

4. Conclusions

The research work presented herein provides a new insight into the analysis of the well-known isotope shift in the atomic spectra of Li using HR-CS-GF-AAS with a modern ML algorithm. Although precision and trueness were one to two orders of magnitude lower than those obtained using MS, the results are metrologically comparable and compatible. The trueness and precision levels allow for the investigation of isotope amount ratios and delta values in naturally occurring samples. A significant advantage of the approach is the lower sensitivity to matrix effects than that of ICP-MS. At least for high Li mass fractions such as in the cathode material, a matrix separation is no longer required, saving time and costs for manpower, reagents, and consumables, as well as a general instrumentational cost reduction. The matrix sensitivity for samples with low Li mass fractions should be tested in follow-up research. HR-CS-AAS combined with ML presents as a fast and low-cost alternative for isotope amount ratio analysis. A better optical resolution capable of resolving the electronic transition $2^2\text{P} \leftarrow 2^2\text{S}$ of Li may improve the accuracy of the isotope amount ratio. Further investigations using these spectrometers are needed to study natural isotopic fractionation. Although the molecular line bands of potentially detectable molecules by flame or HR-CS-GF-MAS (Li_2 , LiH, LiCl, LiBr, and LiI) were found to be too weak,⁴⁵ they deserve further investigation for isotope amount ratio analyses.

5. Acknowledgments

The authors thank the support of Analytik Jena AG on this research with the HR-CS-AAS instrumentation. We are deeply grateful to Daniel Frick from GFZ Helmholtz Centre Potsdam, whose comments and observations enhanced this article.

6. Conflict of interest

The authors declare no conflict of interest.

7. References

- (1) Penniston-Dorland, S.; Liu, X.-M.; Rudnick, R. L. *Reviews in Mineralogy and Geochemistry* **2017**, *82*, 165-217.
- (2) Hathorne, E.; James, R. *Earth. Planet. Sci. Lett.* **2006**, *246*, 393-406.
- (3) Zhang, X.; Saldi, G. D.; Schott, J.; Bouchez, J.; Kuessner, M.; Montouillout, V.; Henehan, M.; Gaillardet, J. *Geochim. Cosmochim. Acta* **2021**, *292*, 333-347.
- (4) Vortmann-Westhoven, B.; Winter, M.; Nowak, S. *Journal of Power Sources* **2017**, *346*, 63-70.
- (5) Okano, K.; Takami, Y.; Yanase, S.; Oi, T. *Energy Procedia* **2015**, *71*, 140-148.
- (6) Diehl, M.; Evertz, M.; Winter, M.; Nowak, S. *RSC Advances* **2019**, *9*, 12055-12062.
- (7) Lui-Heung, C.; Edmond, J. M. *Geochim. Cosmochim. Acta* **1988**, *52*, 1711-1717.
- (8) Tomascak, P. B.; Carlson, R. W.; Shirey, S. B. *Chem. Geol.* **1999**, *158*, 145-154.
- (9) Tomascak, P. B.; Magna, T.; Dohmen, R. In *Advances in Lithium Isotope Geochemistry*, 2016, pp 5-18.
- (10) Lin, J.; Liu, Y.; Hu, Z.; Yang, L.; Chen, K.; Chen, H.; Zong, K.; Gao, S. *J. Anal. At. Spectrom.* **2016**, *31*, 390-397.
- (11) Van Hoecke, K.; Belza, J.; Croymans, T.; Misra, S.; Claeys, P.; Vanhaecke, F. *J. Anal. At. Spectrom.* **2015**, *30*, 2533-2540.
- (12) Kuessner, M. L.; Gourgiotis, A.; Manhès, G.; Bouchez, J.; Zhang, X.; Gaillardet, J. *Geostand. Geoanal. Res.* **2019**, *44*, 57-67.
- (13) Birch, N. J.; Robinson, D.; Inie, R. A.; Hullin, R. P. *J. Pharm. Pharmacol.* **1978**, *30*, 683-685.
- (14) Kragh, H. *Studies in History and Philosophy of Science Part B: Studies in History and Philosophy of Modern Physics* **2012**, *43*, 176-183.
- (15) Cremers, D. A.; Beddingfield, A.; Smithwick, R.; Chinni, R. C.; Jones, C. R.; Beardsley, B.; Karch, L. *Appl. Spectrosc.* **2012**, *66*, 250-261.
- (16) Geisler, S.; Okruss, M.; Becker-Ross, H.; Huang, M. D.; Esser, N.; Florek, S. *Spectrochim. Acta, Part B* **2015**, *107*, 11-16.
- (17) Stevenson, I. C.; Pérez-Ríos, J. *Journal of Physics B: Atomic, Molecular and Optical Physics* **2019**, *52*.
- (18) Walsh, A. *Spectrochim. Acta* **1955**, *7*, 108-117.
- (19) Wheat, J. A. *Applied Spectroscopy* **1971**, *25*, 328-330.
- (20) Chapman, J. F.; Dale, L. S. *Analytica Chimica Acta* **1976**, *87*, 91-95.
- (21) Meier, A. L. *Analytical Chemistry* **1982**, *54*, 2158-2161.

- (22) Kushita, K. *Analytica Chimica Acta* **1986**, *183*, 225-230.
- (23) Smith, B. W.; Gornushkin, I.; King, L. A.; Winefordner, J. D. *Spectrochimica Acta Part B: Atomic Spectroscopy* **1998**, *53*, 1131-1138.
- (24) Wizemann, H. D.; Niemax, K. *Spectrochim. Acta, Part B* **2000**, *55*, 637-650.
- (25) Rehman, E. U.; Rehman, S. U.; Ahmed, S. *Applied Spectroscopy* **2009**, *63*, 971-973.
- (26) Coplen, T. B.; Shrestha, Y. *Pure Appl. Chem.* **2016**, *88*, 1203-1224.
- (27) Bol'shakov, A. A.; Mao, X.; Russo, R. E. *J. Anal. At. Spectrom.* **2017**, *32*, 657-670.
- (28) Resano, M.; Aramendía, M.; Nakadi, F. V.; García-Ruiz, E.; Alvarez-Llamas, C.; Bordel, N.; Pisonero, J.; Bolea-Fernández, E.; Liu, T.; Vanhaecke, F. *TrAC, Trends Anal. Chem.* **2020**, *129*, 115955.
- (29) Nakadi, F. V.; da Veiga, M. A. M. S.; Aramendía, M.; García-Ruiz, E.; Resano, M. *J. Anal. At. Spectrom.* **2015**, *30*, 1531-1540.
- (30) Nakadi, F. V.; da Veiga, M. A. M. S.; Aramendia, M.; Garcia-Ruiz, E.; Resano, M. *J. Anal. At. Spectrom.* **2016**, *31*, 1381-1390.
- (31) Zanatta, M. B. T.; Nakadi, F. V.; Resano, M.; da Veiga, M. A. M. S. *J. Anal. At. Spectrom.* **2019**.
- (32) Abad, C.; Florek, S.; Becker-Ross, H.; Huang, M.-D.; Heinrich, H.-J.; Recknagel, S.; Vogl, J.; Jakubowski, N.; Panne, U. *Spectrochim. Acta, Part B* **2017**, *136*, 116-122.
- (33) Chen, T.; Guestrin, C. In *Proceedings of the 22nd ACM SIGKDD International Conference on Knowledge Discovery and Data Mining*; Association for Computing Machinery: San Francisco, California, USA, 2016, pp 785–794.
- (34) Sheridan, R. P.; Wang, W. M.; Liaw, A.; Ma, J.; Gifford, E. M. *Journal of Chemical Information and Modeling* **2016**, *56*, 2353-2360.
- (35) Guang, P.; Huang, W.; Guo, L.; Yang, X.; Huang, F.; Yang, M.; Wen, W.; Li, L. *Medicine (Baltimore)* **2020**, *99*, e19657-e19657.
- (36) Rosner, M.; Pritzkow, W.; Vogl, J.; Voerkelius, S. *Anal. Chem.* **2011**, *83*, 2562-2568.
- (37) Geilert, S.; Vogl, J.; Rosner, M.; Voerkelius, S.; Eichert, T. *Mass Spectrometry & Purification Techniques* **2015**, *1*, 1.
- (38) Qi, H. P.; Taylor, P. D. P.; Berglund, M.; De Bièvre, P. *Int. J. Mass Spectrom. Ion Processes* **1997**, *171*, 263-268.
- (39) Eigenvector Research, Inc., 2020.
- (40) Mariella, R. *Appl. Phys. Lett.* **1979**, *35*, 580-581.
- (41) Welz, B.; Becker-Ross, H.; Florek, S.; Heitmann, U. *High-Resolution Continuum Source AAS: The Better Way to Do Atomic Absorption Spectrometry*; Wiley-VCH Verlag GmbH & Co. KGaA, 2006, p 296.
- (42) In *ISO/IEC 17043:2010*; International Organization for Standardization: Geneva, 2010.

(43) Vogl, J.; Rosner, M.; Kasemann, S. A.; Kraft, R.; Meixner, A.; Noordmann, J.; Rabb, S.; Rienitz, O.; Schuessler, J. A.; Tatzel, M.; Vocke, R. D. *Geostand. Geoanal. Res.* **2020**, *44*, 439-457.

(44) Vogl, J.; Rosner, M.; Pritzkow, W. *J. Anal. At. Spectrom.* **2011**, *26*, 861-869.

(45) Herzberg, G. *Molecular Spectra and Molecular Structure I. Spectra of Diatomic Molecules*, Second ed.; Van Nostrand Reinhold: New York, 1950; Vol. I. Spectra of Diatomic Molecules.